Anal. Chem. **1996,** *68,* 2966−2973

Spectroscopic Imaging of Laser-Induced Plasma

Valery Bulatov, Liang Xu, and Israel Schechter*

Department of Chemistry, Technion-Israel Institute of Technology, Technion City, Haifa 32 000, Israel

Spectroscopic imaging provides 2D images with full spectral resolution at each pixel. Thus, chemical imaging of an object, as well as other useful information, can be obtained. An imaging spectroscopy method in the visible range is presented and applied to laser plasma. This is a powerful research tool with numerous possible applications. This study is focused on spectroscopic imaging of laser-produced plasmas, and such spectral images (full spectrum at each pixel) are presented for the first time. Detailed information on optical and geometrical effects are obtained, and an insight to the optimization of the laser plasma spectroscopy method is achieved. The size and the spatial shape of the plasma, which can be used for matrix effect compensation, are measured. Similarity maps and classification maps of laser-induced plasma are obtained for the first time. These maps are used for allocation of chemical components in the plasma. The signal to noise ratio maps of the spectra obtained from laser-induced plasmas are provided. These surfaces possess a clear maximum, indicating that there is a preferred site in the plasma, where the emitted light provides the best signal to noise ratio. The performance of the current method is limited by the lack of temporal resolution, although it can be extended by a proper temporal gating.

Imaging spectroscopy provides a new powerful tool for chemical imaging. It combines the analytical power of traditional spectroscopy with two-dimensional (2D) visualization. In this method we obtain a 2D image of an object with full spectrum at each of its pixels. It provides information on chemical composition with spatial resolution. Such a tool can be used for specific analytical applications such as required in several disciplines, e.g., molecular biology and environmental science. Another promising direction is the application of chemical imaging to the improvement of current analytical methods. We present a new imaging method in the visible range that has numerous possible applications. This particular study is focused on the potential of chemical imaging to improve the analytical power of the laser plasma spectroscopy (LPS) method.

Spectroscopic imaging is a relatively new analytical discipline, whose exploration has just started. It is based on modern charge coupled devices (CCD) that are coupled to spectroscopic utilities and to fast data-transfer capabilities. A rather simple instrumentation had been developed previously for imaging fluorescence analysis[1] and has been applied to detect pathological and physiological changes in plants. This method, however, has no spectral resolution since it is based on filters. It can only provide the fluorescence intensities in a 2D plane. A true spectroscopic imaging instrument that is sensitive in the IR range has been recently reported.[2] Imaging in the *visible* range can be carried out by acousto-optic or liquid-crystal tunable filters. Both techniques, however, suffer poor sensitivity due to considerable light loss in these media. Therefore, a preferred approach would be based on Fourier transform visible spectroscopy (FTVS), although it is much more complicated. In this study we present a chemical imaging method that is based on the FTVS technique.

The FTVS method can be applied to a variety of analytical problems. Many promising analytical applications are related to microbiology and environmental monitoring. In this study we focus on such a method, namely, LPS. In this well-established method, a laser pulse is focused onto a sample to produce a small plasma plume.[3−22] The hot plasma (∼25 000 °C) ablates a small part of the substrate and excites its atoms. The light emission that originates from the decay of the atoms to ground state is used for chemical identification and quantification.

Laser plasma imaging has been recognized as a powerful research tool.[23] In most cases imaging has been achieved by fast framing photography,[24] by streak cameras,[25,26] and by ICCD

(1) Ning, L.; Edwards, G. E.; Strobel, G. A.; Daley, L. S.; Callis, J. B. *Appl. Spectrosc.* **1995**, *49*, 1381−9.
(2) Lewis, E. N.; Treado, P. J.; Reeder, R. C.; Story, G. S.; Dowrey, A. E.; Marcott, C.; Levin, I. W. *Anal. Chem.* **1995**, *67*, 3377−81.
(3) Moenke-Blankenburg, L. *Laser Microanalysis*; Wiley: New York, 1989.
(4) Leis, F.; Sdorra, W.; Ko, J.-B.; Niemax, K. *Mikrochim. Acta II* **1989**, 85−199.
(5) Sdorra, W.; Quentmeier, A.; Niemax, K. *Mikrochim. Acta II* **1989**, 201−19.
(6) Radziemski, L. J.; Cremers, D. A. In *Laser-Induced Plasmas and Applications*; Radziemski, L. J., Cremers, D. A., Eds.; Marcel Dekker: New York, 1989.
(7) Wisbrun, R.; Niessner, R.; Schröder, H. *Anal. Methods Instrum.* **1993**, *1*, 1−5.
(8) Wisbrun, R.; Schechter, I.; Niessner, R.; Schröder, H. *Proc. Int. Soc. Opt. Eng.* **1992**, *1716*, 2−15.
(9) Wisbrun, R.; Schechter, I.; Niessner, R.; Schröder, H.; Kompa, K. L. *Anal. Chem.* **1994**, *66*, 2964−75.
(10) Schechter, I.; Wisbrun, R.; Niessner, R.; Schröder, H.; Kompa, K. L. *Proc. Int. Soc. Opt. Eng.* **1994**, *2092*, 174−85.
(11) Schechter, I.; Wisbrun, R.; Niessner, R.; Schröder, H.; Kompa, K. L. *Proc. Int. Soc. Opt. Eng.* **1994**, *2093*, 310−21.
(12) Schröder, H.; Schechter, I.; Wisbrun, R.; Niessner, R. In *Excimer Lasers: The Tools, Fundamentals of their Interactions with Matter, Fields of Applications*; Laude, L. D., Ed.; Kluwer Academic Publishers: New York, 1994; pp 269−87.
(13) Schechter, I. *Anal. Sci. Technol.* **1995**, *8*, 779−86.
(14) Sdorra, W.; Niemax, K. *Mikrochim. Acta* **1992**, *107*, 319−27.
(15) Beauchemin, D.; Le Blanc, J. C. Y.; Peters, G. R.; Craig, J. M. *Anal. Chem.* **1992**, *64*, 442R−67R.
(16) Cates, M. C. *Proc. Int. Soc. Opt. Eng.* **1990**, *1279*, 102−11.
(17) Thompson, M.; Chenery, S.; Brett, L. *J. Anal. At. Spectrom.* **1990**, *5*, 49−55.
(18) Niemax, K.; Sdorra, W. *Appl. Opt.* **1990**, *29*, 5000−6.
(19) Sdorra, W.; Niemax, K. *Spectrochim. Acta* **1990**, *45B*, 1917−26.
(20) Majidi, V.; Joseph, M. R. *Crit. Rev. Anal. Chem.* **1992**, *23*, 143−62.
(21) Majidi, V. *Spectroscopy* **1993**, *8*, 16−24.
(22) Xu, N.; Majidi, V. *Appl. Spectrosc.* **1993**, *47*, 1134−9.
(23) Chrisey, D. B., Hubler, G. K., Eds.; *Pulsed Laser Deposition of Thin Films*; John Wiley & Sons: New York, 1994.
(24) Scott, K.; Huntley, J. M.; Phillips, W. A.; Clarke, J.; Field, J. E. *Appl. Phys. Lett.* **1990**, *57*, 922.

S0003-2700(96)00277-6 CCC: $12.00

detectors.[27−29] It has been applied for numerous basic studies of laser ablation processes, such as time-resolved spatial distribution. These studies, however, were not both spectrally and spatially resolved simultaneously. In another study, full laser plume spectra have been obtained as a function of the distance from the ablated surface, by an optical setup that has focused a slice of the plume image into the spectrometer.[30] The main observation obtained with this setup has been that as the distance from the surface is increased the continuum fluorescence intensities of the emission spectra decrease with an increase in the relative intensities of the discrete lines which prominently merge. The main conclusion of that study has been that the plasma plume is highly nonhomogeneous in its composition and temperature as a function of distance from the surface. This conclusion suggests that a 2D imaging, with full spectral resolution at each pixel, is of considerable importance.

LPS analysis has several advantages over many other traditional methods. The most important is the capability to perform direct solid analysis, without the need of chemical preparations. It can provide simultaneous analysis of many elements, and only optical access to the analyzed material is required. Due to its simplicity, this method can be easily developed as on on-line and in situ analytical technique, e.g., refs 7−13. Actually, this method has most of the qualifications that are needed in environmental monitoring, and such applications have already been developed, e.g., ref 9.

In spite of the above advantages, the LPS method has not yet reached the best sensitivity that is required in the most demanding environmental analyses. The current detection limits are in the range of 10 ppm (based on 95% confidence intervals) or 1 ppm (based on 3σ).[9] An interesting question is the reason for this relatively poor performance, and whether it is possible to achieve a significant improvement of the sensitivity. In order to refer to these questions, we compare the LPS method to the best elemental analytical method, namely, to the ICP method. In both methods plasma is used for excitation and the emitted light is the bases of analysis. However, ICP provides detection limits in the sub-ppb, while LPS in the ppm range. The major difference between these two plasma techniques is that the ICP uses very stable plasma, while LPS, due to its very nature, is based on unstable plasma and depends on nonlinear ablation processes. The second important difference is that ICP usually takes homogenized liquid samples while LPS is used for direct solid analysis.

The conclusion that can be drawn from the above comparison is that there is a chance to improve the sensitivity of LPS, provided that we overcome the problems due to instabilities of the plasma. The instability of the plasma is an intrinsic property of this method; however, we can compensate for it by a proper characterization of the plasma. We need more information about the plasma in order to compensate for matrix effects and in order to optimize the optical measurements. Our task in this study has been to gain the required information on the plasma in the LPS method, which has the potential to improve its performance. Imaging spectroscopy can provide information on the size of the plasma, on its spatial shape, and on its temperature, properties that are closely related to matrix effects and to the actual ablation process.

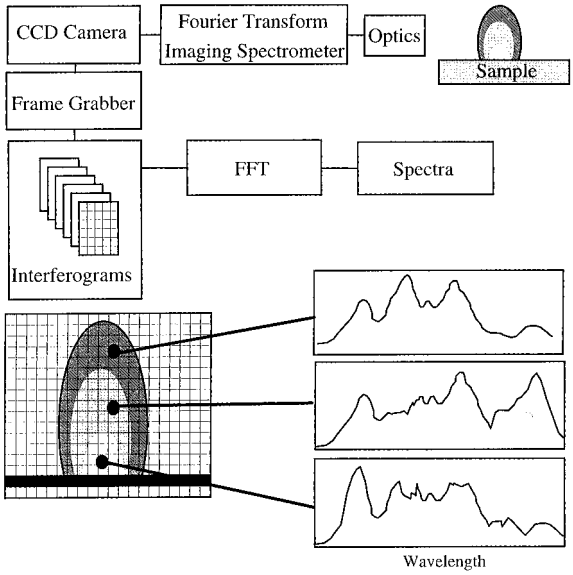

Figure 1. Schematic electro-optical setup for imaging with Fourier transform visible spectroscopy. Spectrum at each pixel is obtained.

Moreover, imaging spectroscopy may provide information on the internal distribution of the elements within the plasma. It might be that, in a way which is similar to ICP, each element or spectral line should be monitored at a preferred location in the plasma. Such information has improved the performance of the ICP method, and it might also improve the LPS analysis. In the following we describe such measurements and demonstrate the powerful information that is gained from chemical imaging of laser-induced plasmas.

EXPERIMENTAL SECTION

Plasmas were produced by a Q-switched Nd:YAG laser that delivers 600 mJ in 7 ns at 1064 nm (Continuum Surelite II). The laser was focused onto various samples by quartz lenses. Most of the measurements were carried out with a lens of $f = 400$ mm; however, also other lenses were used in order to study the effect of focusing conditions.

The laser beam area was 1 cm^2 (86 MW cm^{-2} at laser output). The actual energy density at the target was varied, according to the particular focusing conditions. The spot diameter was changed from ∼200 μm to 0.7 mm; thus, target energy density changed from 270 GW cm^{-2} to 220 MW cm^{-2}.

The electro-optical setup for imaging with FTVS is described in Figure 1. It consists of imaging optics (zoom lenses) coupled to a step-scan FTVS. This instrument is based on a mechanically driven interferometer, coordinated with a CCD camera. In this way an image is collected for each step of the interferometer. The interferograms are imaged onto a thermoelectrically cooled frame-transfer CCD camera (from Princeton Instruments). The interferometer steps were fitted to the maximum data acquisition rate of the CCD (in its frame-transfer mode of operation). The imaging spectra are obtained from these interferograms by a common FFT algorithm. This system provided spectral intensities with 12 bit accuracy, for ∼100 wavelengths in the range of 400−800 nm. This spectral information is provided for each of the 100 × 100 CCD pixels.

Most of the examined samples were alloys of known compositions, although other samples, such as locally collected stones,

(25) Dyer, P. E.; Sidhu, J. *J. Appl. Phys.* **1988**, *64*, 4657.
(26) Eryu, O.; Murakami, K.; Masuda, K.; Kasuya, A.; Nishina, Y. *Appl. Phys. Lett.* **1989**, *54*, 2716.
(27) Cappelli, M. A.; Paul, P. H.; Hanson, R. K. *Appl. Phys. Lett.* **1990**, *56*, 1715.
(28) Gupta, A.; Braren, B.; Casey, K. G.; Hussey, B. W.; *Kelly*, R. *Appl. Phys. Lett.* **1991**, *59*, 1302.
(29) Geohegan, D. B. *Appl. Phys. Lett.* **1993**, *62*, 1463.
(30) Hoffman, A.; Manory, R.; Bourdillon, A.; Paul, G. L. *Supercond. Sci. Technol.* **1990**, *3*, 395−403.

were studied as well. Each analysis consisted of ~10 laser pulses at each interferometer step. Thus, the interferograms are averaged over accidental fluctuations. The CCD camera collected the emitted light at a repetition rate that was matched to the laser firing rate (actually the laser was driven at the predefined rate of the camera). In this operational mode, a full 100 × 100 imaging spectrum could be collected in a few minutes.

The results of the above experimental setup are multidimensional data; thus, reductions are required for their presentation. We present results in two different representations: In the first way, we convolute the spectra with human eye sensitivity, which results in colored 2D images. Such images represent what the human eye could observe if plasma were frozen. These figures are then gray-scaled for publication. In the second representation, we use regular 3D mesh plots: The X and Y coordinates represent the real spatial coordinates, while the Z axis represents the integrated intensity at a point in the $X-Y$ plane. Integration is carried out over the whole spectral rage (400−800 nm). This intensity in coded by a regular color scale, where the blue corresponds to the lowest intensity and the red to the highest one. These 3D colored plots are then rescaled to gray levels for publication.

Computer programs for data analysis were written in FORTRAN and compiled with an MS-FORTRAN Power Station compiler. All codes were run on PC (486 and Pentium processors).

RESULTS AND DISCUSSION

We first studied several optical and geometrical effects and then focused on the chemical imaging of the plasma.

Lens Effect. We studied the effect of the lens used for focusing the laser beam onto the sample. Each lens produces a different energy density distribution in space, resulting in different plasma characteristics. This effect has never been studied systematically, although much experimental evidence is available.[9] It is commonly believed that too hard focusing conditions (small focal length) do not provide good results. Usually, relatively soft focusing (using a lens with a long focal length) is preferred, in part because in such conditions the exact location of the sample along the laser beam coordinate is not of considerably importance.

In order to understand the lens effect, we have created the image of the plasma obtained by a variety of lenses, of different focal length. In each case the sample has been placed at the focus. Laser plasmas are known to be highly dependent on the laser power density at the surface and vary significantly for a single lens; therefore, laser characteristics have not been changed in this experiment. Power densities for each lens can be directly derived from the laser beam profile (described in the Experimental Section) and the focal length. The results are shown in Figure 2, where the target was a metal Cu foil. We can see that the lens of $f = 150$ mm produces a very small and hot plasma, due to the high energy density that is localized at the focal point. This is the reason for the well-known poor analytical performance obtained under such conditions. On the other hand, the lens of $f = 1000$ mm is also not suitable for analytical purposes, due to the long "tail" along the laser beam. The best conditions are obtained at $f = \sim 400$ mm. The plasma "tail", which is clearly observed at long focal length but is also present at medium focusing conditions, originates from the laser pulses producing an aerosol above the sample. The next pulse is partially scattered by these aerosol particles. At $f = 1000$ mm a considerable part of the energy is scattered and only a too-small portion of the energy reaches the surface of the sample. This results in a poor analytical performance. On the other hand, the same aerosol effect contributes to an *improvement* of the results at medium focusing conditions, where the energy density (at the same distance from the surface) is lower: In this case, less light is scattered, and the persistent aerosol is excited in the hot plasma to produce good analytical spectral lines. This aerosol is composed of substrate material and produces the right spectral lines without the need to spend energy on surface ablation. This effect was previously observed and quantified,[9,13] and here we provide an explanation based on the imaging of the plasma. As previously shown,[9,13] the long emission tail obtained under similar conditions

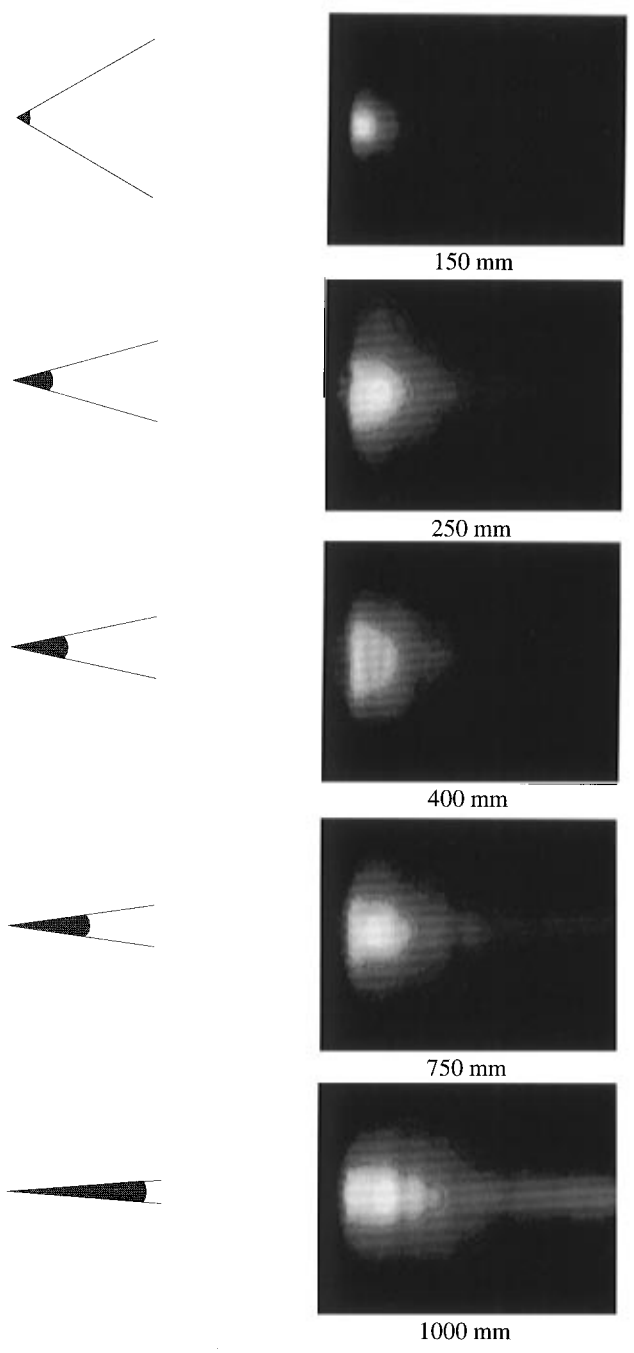

Figure 2. Study of the effect of the lens on the induced plasma. Each focusing condition results in different plasma characteristics. Conical volumes bounding energy density up to a definite value are schematically plotted on the left.

originates from residual particles. This explanation is probably correct in this particular case as well, since both laser characteristics and sample have been kept fixed. Generally, a long tail can be established also by using a short focal length lens if the power density is reduced, and the results depend on the sample properties as well. The detailed plasma expansion dynamics depend on almost all experimental conditions, and its study is outside of the purpose of this research.

At an even longer focal length (not shown) the high energy density that is needed for plasma formation is reached already much ahead of the surface of the sample. Therefore, plasma is created in air, far away from the sample. Much energy is lost ahead of the observation volume, thus considerably reducing the analytical performance.

Sample Location. Another experimental parameter that was optimized empirically, and now can be understood on the basis of the imaging, is the location of the sample relative to the focus of the lens.[9] The general knowledge is that placing the sample somewhat in front or behind the focus provides better results. In order to understand this effect, we have plotted the image of the plasma obtained by the same lens ($f = 400$ mm); however, each time the sample has been placed at a different distance.

The results are shown in Figure 3. When the sample is placed too close to the lens, the plasma is very flat and relatively cold. In this case, the plasma cannot be induced in the air and is induced solely by the surface material. As we move the sample toward the focus, the plasma becomes more spherical and the results are better. The details of these figures can be understood in terms of fluence and spot size; however, only qualitative explanations are provided here. The best conditions are obtained when the plasma is induced in the air just in front of the sample. When the sample is placed in the focus exactly, a hot ring around the main plasma plume is formed, which reduces the analytical performance. This ring can be clearly observed at the bottom of Figure 3. It probably originates from scattered material. This picture is supported by the shape of the laser craters that were previously published[3−6] and that indicate material scattering at an angle of 30−45°.

Similarity Maps. Once the images of the plasma are available, their internal structure should be investigated. First, we want to study similarities within each image, namely, regions that have similar spectral characteristics. For this purpose we have drawn similarity maps that identify similarities between each pixel of the image and a reference spectrum at a defined pixel. The intensity, I_{xy} at each point $\{x, y\}$ of the similarity map has been calculated by

$$I_{x,y} = [\int_{\lambda_1}^{\lambda_2} |S_{x,y}(\lambda) - R(\lambda)|\, \mathrm{d}\lambda]^{-1}$$

were $S_{x,y}(\lambda)$ is the spectrum at $\{x, y\}$ and $R(\lambda)$ is the reference spectrum.

Such similarity maps are shown in Figure 4. The image of the plasma is shown at the upper left corner, together with a set of seven reference points. These points indicate the location of the reference spectra used to form the similarity maps. (Full spectra have been used as references in these figures; however, particular spectral lines can be used as well.) The other seven images in Figure 4 present the similarity maps, each of them created for a different reference spectrum (as defined by the points).

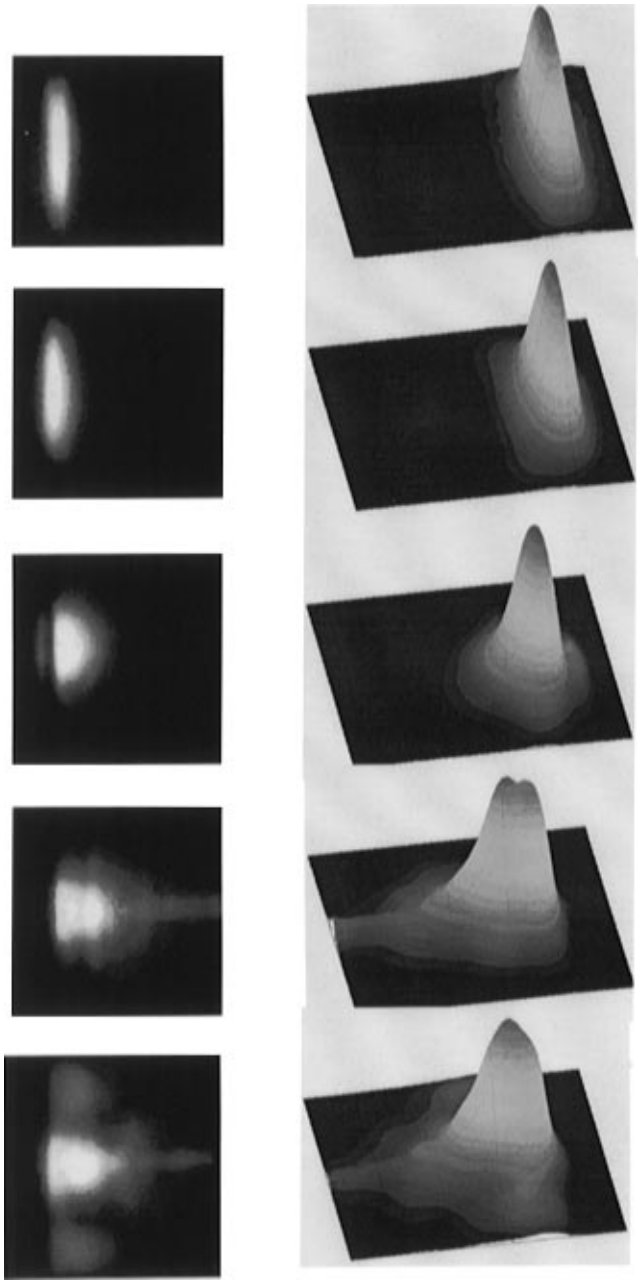

Figure 3. Effect of the location of the sample along the laser beam. The sample was located in front of the focal point, at the following distances from the focus (from top to botton): 260, 150, 40, 15, and 0 mm. Since a lens of $f = 400$ was used, the distances of the target from the lens were 140, 250, 360, 385, and 400, (from top to bottom).

The most important feature observed in these maps is the general spherical symmetry of the plasma. This is of importance since this feature enables calculations of the spectra as a function of the distance from the center: We have to take into account that these 2D images represent 3D objects, and the deconvolution can be carried out by the Abel algorithm, only under the assumption of a certain level of spherical symmetry.[31] In addition we see that the composition of the "tail" is mostly similar to the outer shell of the plasma.

Obviously, these maps depend of the focusing conditions and on other geometrical parameters of the experimental setup. The above measurements, however, have been carried out at the optimized and common conditions.

Spectral Windows. Since we obtain the full spectrum at each pixel, we can draw the image of the plasma at any desired

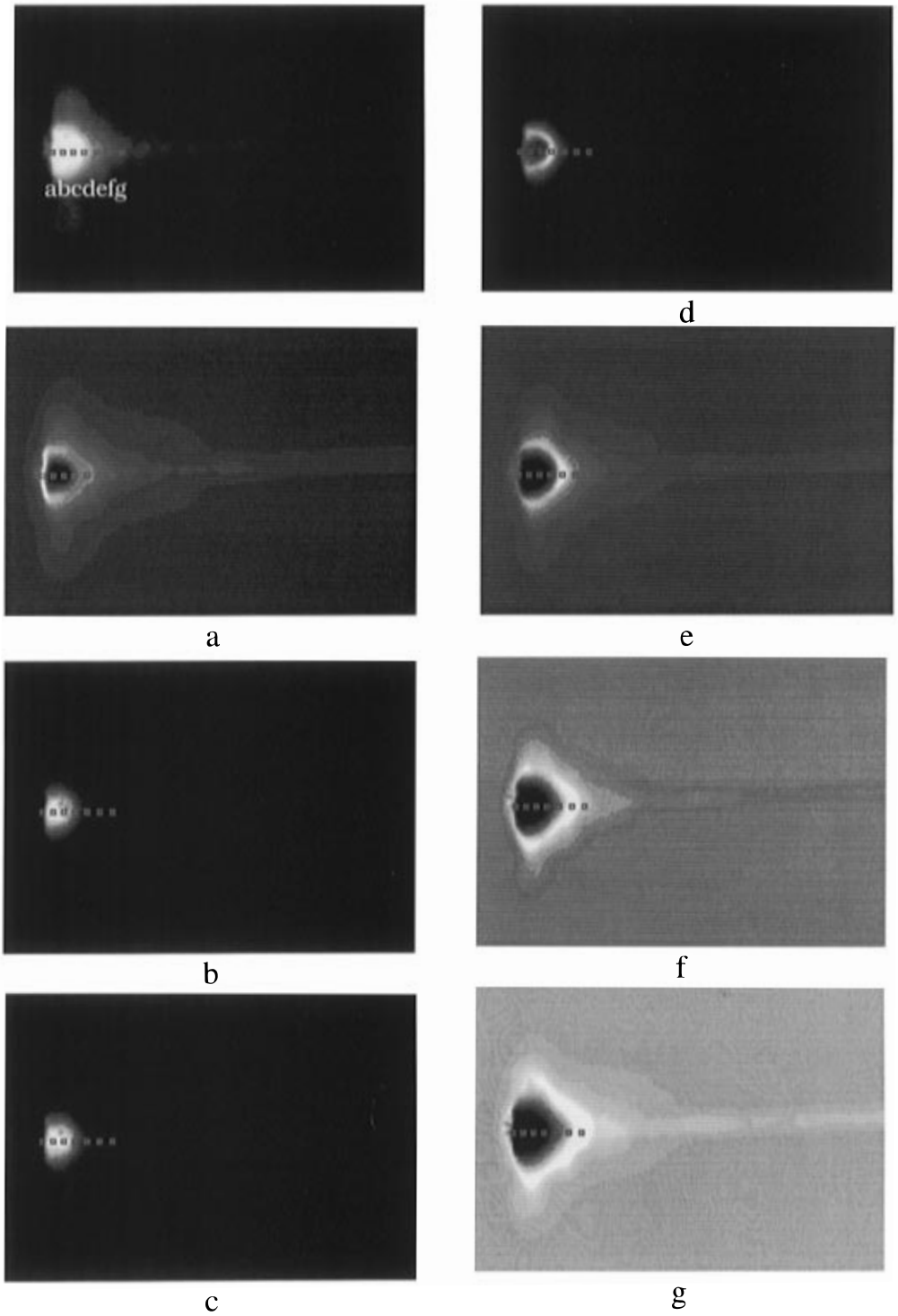

Figure 4. Similarity maps of the plasma. The laser beam focused by a lens of $f = 400$ mm onto a brass sample. The original image of the plasma is shown at the top left corner, together with seven reference points (along the laser beam). Panels a−g are the similarity maps of the original plasma, calculated with respect to the reference spectra at points a−g. Note the spherical symmetry of the plasma.

wavelength. We induced the plasma onto a brass sample. Figure 5 presents the image of the plasma at the full spectral rage (400−800 nm) and at four selected wavelengths: two lines of Zn (481 and 636 nm) and two lines of Cu (522 and 578 nm). The 3D representation has been shown in this figure. It can be seen that, generally, Cu is located at the center of the plasma, while Zn is more in the outer shell. Moreover, each wavelength has a different spatial shape that probably originates from the differences in transition energy and distribution of temperature in the plasma. These findings provide more detailed chemical information as compared to previous studies on spatial distribution of species in laser plasmas.[23] Nevertheless, a more profound study is needed for understanding the details of these images.

Classification Algorithm. In order to visualize the location of several components in the plasma, it is useful to create classification maps. Such maps should classify the image in respect to several known reference spectra of pure components. There are many possible classification algorithms. Among the most common algorithms are the principal component analysis (PCA) and the least-squares linear combination (LSLC); however,

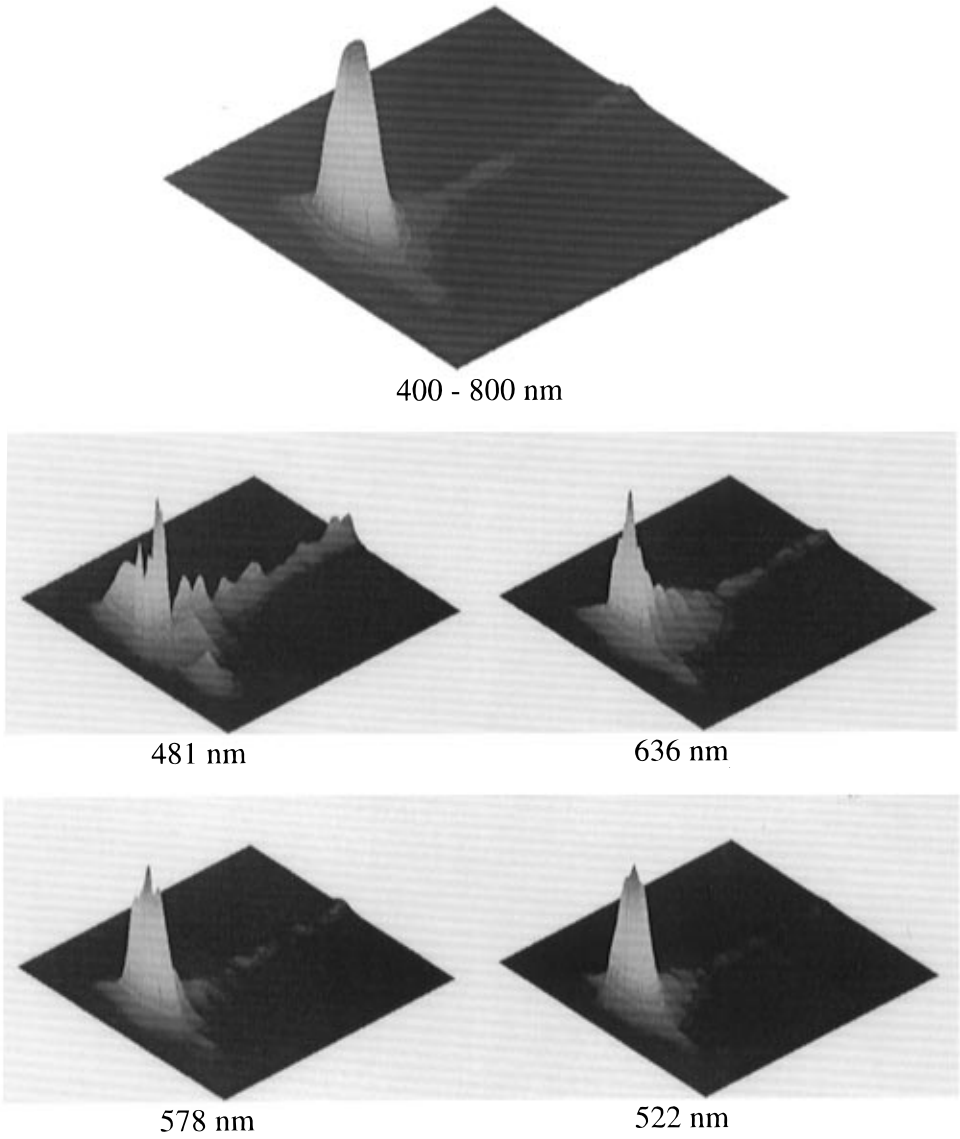

Figure 5. A 3D representation of the integrated intensities of the full spectral image of the plasma (top) and of the images obtained by application of "logical" filters at several emission wavelengths (four bottom images).

other methods are also acceptable. In the following we use the LSLC algorithm.

The classification map is formed in the following way: The spectrum at each pixel in the image, $S_{x,y}(\lambda)$, is described as a linear combination of the reference known spectra of pure components, $R^1_{x,y}(\lambda)$ and $R^2_{x,y}(\lambda)$ (two references in this example):

$$S_{x,y}(\lambda) = \alpha R^1_{x,y}(\lambda) + \beta R^2_{x,y}(\lambda)$$

where α and β are parametric coefficients obtained by least-squares fitting. These coefficients are the basis of classification, and the presence of a component at a pixel $\{x, y\}$ is decided by the highest coefficient at that pixel. This representation allows only one component at each pixel, the one that has a larger coefficient. (Color representations allow for a mixture of components at each pixel, according the ratio of their fitting coefficients.)

Using a gray scale, we can present clearly only a few components. Presentation of classification maps of many components is best obtained with colors, where a separate color represents each component. Such gray-scaled classification maps are shown in Figure 6, where the two components are Zn and Cu. In this case we actually used three reference spectra: the pure spectra of the two elements and the black-body spectrum that could describe the hottest areas. Each of the maps has been obtained under different focusing conditions. The reference spectra of pure components have been obtained from plasma of pure samples (actually measured by another experimental setup, namely, by an intensified photodiode array spectrometer).

Generally, these maps show that Zn is present at an *outer* shell and in the "tail" of the plasma, while Cu is present mainly in an *inner* shell. This feature is in agreement with the physcial intuition, since the melting point of Zn is lower. At the very center of the plasma the spectra are noisy (due to the high temperature), and the parametric coefficients of both elements are very small. The upper map was obtained at the optimum conditions ($f = 400$ nm). The next map (from top to bottom) was obtained with $f = 1000$ mm. In this case the energy density is higher, and a larger volume is classified as Cu. The next map was obtained with $f = 400$ mm also; however, the sample was located just at the focus.

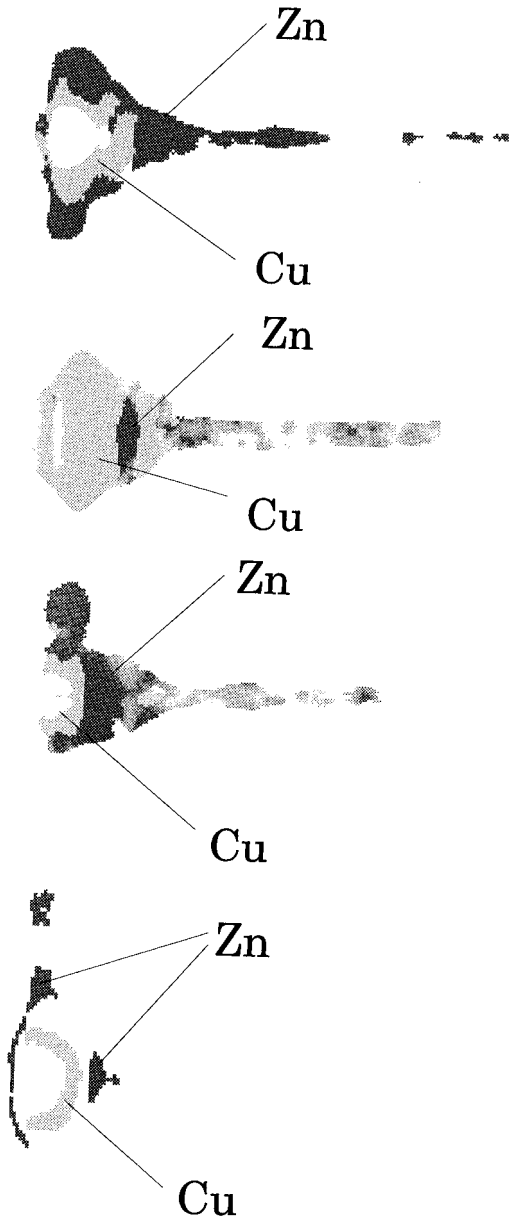

Figure 6. A result of the classication algorithm. Each image is collected at different focusing conditions; however, in all cases Cu is located at an inner shell while Zn is at an outer shell. A lens of $f =$ 400 mm was used, and the distances of the target from the lens were 400, 385, 360, and 250 mm (from top to bottom).

Here the plasma is relatively localized, but some material is sputtered away. The bottom map was obtained with a lens of $f =$ 150 mm. The plasma is small and hot, and only a thin shell of Cu and some residuals of Zn are observed. This is probably the reason for the poor analytical performance at such conditions.

The above classification maps are calculated using full reference spectra. It would be interesting to present classification maps where the reference is a particular spectral line (transition). Such maps could provide interesting insight into the spatial distribution of energy states in the plasma. Unfortunately, the current data are not suitable for such detailed information. Our spectral information is time-integrated and is of relatively broad spectral resolution; thus, spatial classification according to single lines is not currently possible.

Signal to Noise Maps. The analytical performance is determined by various factors, one of the most important being the spectral signal to noise ratio (S/N). Therefore, maps of the S/N are of relevance. We have calculated these values at each pixel to obtain such maps. The S/N values were based on the intensities of identified spectral lines and on intensities of weak lines that fluctuate (close to zero average). These maps can be presented as mash surfaces in a 3D plot (*X* and *Y* represent the actual location, and *Z* represents the S/N values). The original surfaces look very spiky and are not useful for drawing general conclusions. However, we have smoothed these surfaces, and such a representative result is shown in Figure 7. (The origin and the direction of the coordinates are defined in the inset.) This surface is still somewhat spiky; however, the general trends are clear. The best S/N can be obtained along the *X* coordinate (along the laser beam), but not too close to the center of the plasma. There are usually several maxima along this coordinate, and then the S/N values decay again. When moving along the *Y* coordinate, one can also observe a maximum; however, this maximum is much lower as compared to the previous one.

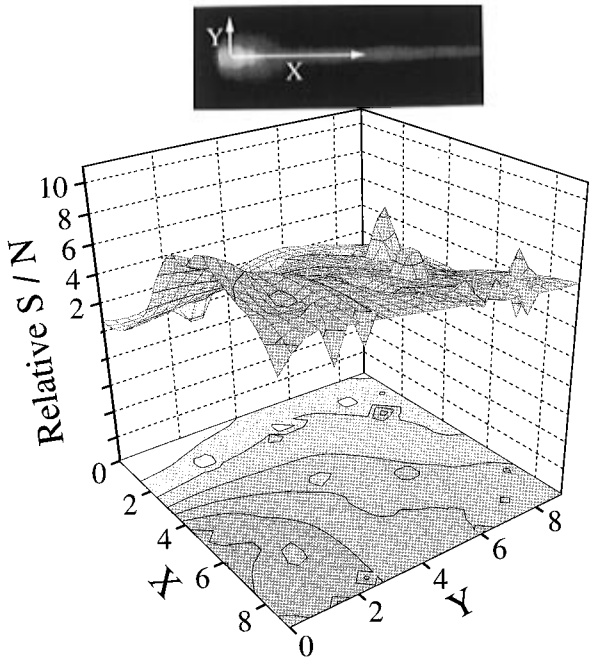

Figure 7. Relative S/N as a function of spatial (*X* and *Y*) coordinates (as defined at the top). Only a quarter of the *X*−*Y* plane is presented. The best measurement site is clearly observed along the *X* coordinate (the laser beam direction), in front of the focal point.

The clear maximum in such maps of the S/N indicates that analysis could be improved by a proper optical setup that is designed to collect the light emitted from the best location. Obviously, the shape of such surfaces depends on many experimental parameters, and more detailed research is needed in order to find out the location of the maximum S/N value as a function of the experimental conditions. However, the presence of such a maximum indicates that optimization is feasible.

CONCLUDING REMARKS

We have presented for the first time chemical imaging of laser-produced plasmas (obtained by 2D full spectroscopy). This powerful tool is proven to provide detailed information that can be used to optimize the experimental setup and to improve analytical performance. Plasma imaging provided insight into the effects of several factors that affect LPS performance, such as the

focusing conditions. Similarity and classification maps proved for the first time that each element is mainly present at a different location in the plasma. We have also found the optimum site in the plasma that provides the best spectral signal to noise ratio.

The above achievements, however, should be considered as preliminary results only. The reason is that there are many other related studies that can and should be carried out in the future, which might result in a deeper understainding of the LPS method. This preliminary study has just presented the research tool and exemplified its potential in LPS analysis. It is noteworthy that most of the results might be very specific to the particular laser and sample conditions. The most important conclusion of this study is that imaging spectroscopy has the potential to considerably improve LPS results. This conclusion is supported by previously studies as well.[30]

The main limitation of the current method is the fact that it provides time-integrated information. It is well-known that LPS performs best in time-gated experimental setups. The reason is that the spectral signal to noise ratio reaches its maximum at a certain delay after the laser pulse (a few microseconds) and for a certain integration time.[9] Time-averaged data are influenced by the initial plasma, which is too hot for analytical purposes. Therefore, the next obvious step will be to study the time-resolved spectroscopic imaging of laser-induced plasma. An experimental setup that will have such capabilities is under construction, although it is much more complicated.

(31) Bekefi, G., Ed. *Principles of laser plasmas*; John Wiley & Sons: New York, 1976.

ACKNOWLEDGMENT

This study was supported by the Committee for Research and Prevention in Occupational Safety and Health and the VPR Fund, Technion-Israel Institute of Technology.

Received for review March 20, 1996. Accepted May 17, 1996.[⊗]

AC960277A

[⊗] Abstract published in *Advance ACS Abstracts,* July 1, 1996.